PROCEEDINGS, 42nd Workshop on Geothermal Reservoir Engineering
Stanford University, Stanford, California, February 13-15, 2017
SGP-TR-212

High-resolution Shallow Structure Revealed with Ambient Noise Tomography on a Dense Array

Xiangfang Zeng, Clifford Thurber, Herb Wang, Dante Fratta, Eric Matzel, PoroTomo Team

1215 West Dayton St., Madison, WI, 53706

zengxf@geology.wisc.edu

Keywords: Brady Hot Springs, Ambient noise tomography, Distributed Acoustic Sensing

ABSTRACT

In March 2016, the PoroTomo Team deployed a dense seismic array to image the structure of the Brady Hot Springs geothermal reservoir in Nevada. At this site, a 4 km by 1.5 km elliptical subsidence area was observed by analyzing InSAR images (Ali et al., 2016). The array was composed of 244 short-period, three-component geophones and ~8,600 m of distributed acoustic sensing (DAS) fiber-optic cable installed in surface trenches plus ~350 m installed in a borehole. The geophone array provided about 60 m spatial sampling whereas sampling of the surface DAS was nominally 1 m. The acquisition system provided 15 days of continuous records that were used to calculate noise cross-correlation functions (NCFs). NCF cans be treated as empirical Green's functions and used in ambient noise tomography. The surface wave dispersion curves were obtained from the NCFs between geophones pairs and pairs of DAS channels. The dispersion curves were inverted for shear wave velocity profiles in different locations of the array. A low velocity zone is associated with the area of subsidence obtained from InSAR.

1. INTRODUCTION

The geothermal field and plant at Brady Hot Springs, Nevada has been generating electrical power for more than 20 years. At the geothermal field, InSAR images have documented the presence of a 4 km by 1.5 km elliptical subsidence area and the depth of the subsidence source was estimated to be not deeper than 600 m (Ali et al., 2016). In March 2016, a dense seismic array was deployed including 244 traditional three-component geophones and ~8,600 m of DAS cable installed in surface trenches and ~350 m of DAS cable installed in a borehole (Figure 1). The typical spacing between geophone stations was about 60 m whereas the spatial interval of the DAS array was nominally 1 m. This array was designed to allow the use of active-source and ambient noise techniques to image the reservoir and reveal the mechanical properties of the rocks in the reservoir (Feigl and PoroTomo, 2017). This information is desirable for optimizing the operation of the enhanced geothermal systems. The active source was a 440-kN force vibroseis truck that occupied 191 locations within and outside the array during the four stages of the experiment. Ambient noise tomography obtained with geophone/seismometer data has been widely used at various scales to image geological structures (e.g., Campillo and Roux, 2014). This technique is based on the interpretation of dispersion curves obtained from NCFs between pairs of seismic sensors (i.e., the inter-station empirical Green's function). Zeng et al. (2016) found that ambient noise tomography using DAS data is practical too. In this study, we use ambient noise tomography with combined geophone and DAS data to image the shallow seismic structure at Brady Hot Springs, Nevada.

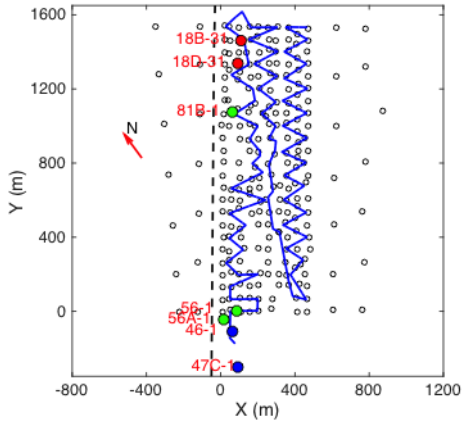

Figure 1: Map of sensors and wells at Brady Hot Springs. The surface DAS cable is shown by the blue line, whereas geophones are denoted with black open circles. The injection, production, and observation wells are indicated with red, blue, and green solid circles. A ~ 350 m long DAS cable was installed in the Well 56-1. Highway I-80 is denoted with a dashed line.

2. DATA AND METHOD

Our data processing includes single station data preparation and station-pair cross-correlation steps (Bensen et al., 2007). Since the data recording systems of the geophones and DAS are quite different from each other, some minor changes were required.

The continuous data of the three-component geophones were stored in one-day long files. The one-day long records were filtered and resampled to 100 Hz and the one-bit normalization method was adopted to reduce the effect of strong signals (e.g., earthquake signals, traffic signals or active source signals). Spectral whitening was also applied between 0.2 and 5 Hz. The processed continuous data were chopped into 10-minutes long segments and used to compute NCFs. Since our whitening frequency band is lower than that of the active source, which was operated during daytime, and the one-bit normalization highly reduced strong transient signals, we were able use the entire day of data to compute the NCFs. The phase weighted stacking (PWS) method has shown potential to improve signal-to-noise ratio significantly but with heavy computational cost (Zeng et al. 2016). Therefore, a hybrid-stacking scheme was introduced to improve computational efficiency, for which the PWS method was used to stack average traces of every ten NCFs instead of all traces. Based on our tests, this approach produces almost identical results with only one-tenth of the computational cost.

The DAS system stored waveforms of 8,671 channels during a 30-second time window per file. The original sampling rate is 1,000 Hz that is far beyond our frequency band of interest and we only calculated the NCFs between channels within a given linear segment. Records of channels in one segment were extracted from the original data file and filtered and resampled to 100 Hz. The dense spatial sampling afforded by DAS made it possible to extract higher frequency signals from ambient noise. The frequency band of whitening was changed to between 5 and 15 Hz and the length of the cross-correlation time window was set to 60 seconds. The new higher frequency band overlaps the swept-frequency active sources, which were operated during daytime. Therefore, we only used 10 hours of nighttime continuous records in the DAS NCF computation.

3. RESULTS

3.1 NCFs of Geophone Data

In total, 28,203 vertical-to-vertical (ZZ) NCFs were obtained. Figure 2 shows a record section of NCFs between geophones pairs along a line parallel to highway I-80. The Rayleigh wave signal clearly emerges on the NCFs and shows a clear move-out. The frequency time analysis technique based on multiple filters was employed to measure group velocity. As shown in Figure 2, the group velocities were picked at the arrival of strongest energy at each frequency. The measurements with low signal-to-noise ratio (SNR) were removed. About 15 thousands dispersion curves were obtained in total. Most measurements are between 2 and 6 Hz. The typical depth of peak sensitivity of a surface wave is about one-third to half of the wavelength. Considering the average group velocity at 4 Hz is ~ 400 m/s, dispersion curves between 2 and 6 Hz reflect shear-wave seismic structure for depths of a hundred to a few hundred meters. To investigate spatial variation, the average group velocities were calculated at a given frequency from NCFs from each station to all nearby stations. This approach produces spatially smoothed estimates of the heterogeneous structure. The low velocity area is consistent with location of the subsidence area obtained from InSAR analysis (Figure 2). There are tens of fumaroles in this area and the surface temperature is higher as shown by the surface Distributed Temperature Sensing array collocated along the horizontal DAS array. These results suggest the presence of near surface fractures in the low velocity area along the Bradys fault trace. One possible explanation of subsidence during geothermal production is sediment compaction due to decreasing pore pressure or desaturation (Ali et al., 2016), which also suggests high-density fractures. The trench exposure across the Bradys fault also reveals high-density fractures in fault zone (Wesnousky et al., 20015). Since high porosity and temperature can significantly decrease seismic velocity, the observed low velocity area might be caused by a combination of both factors.

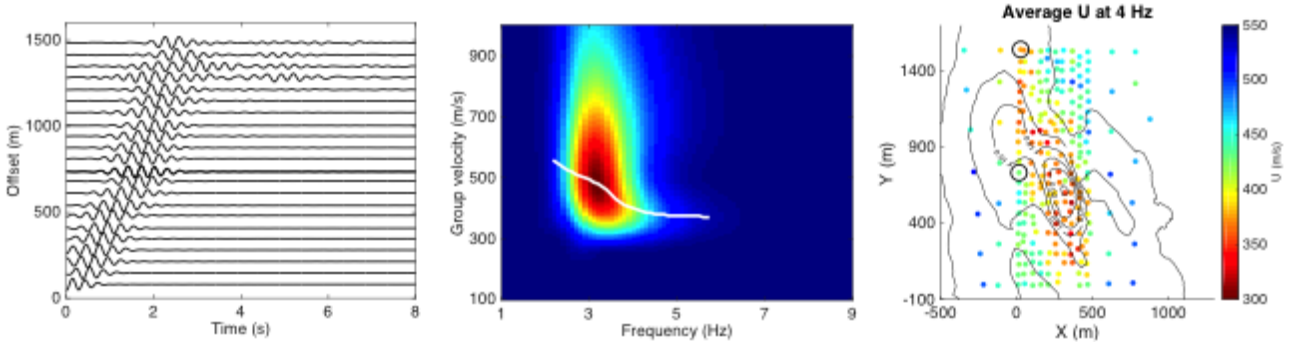

Figure 2. (Left) The symmetric components of NCFs between N207 and other stations parallel to highway I-80. (Middle) Frequency-time analysis diagram of NCF between N207 and N196 geophones (circles in the bottom panel). The picked group velocities are shown in white line and color represents amplitude of envelopes of filtered waveforms. (Right) Average group velocity around each station at 4 Hz. Color corresponds to velocity and contour lines represent subsidence between 12/24/2011 and 10/27/2012 in meter (Ali et al., 2016).

3.2 NCFs of DAS Data

Figure 3 shows an NCF record section along a segment that is perpendicular to highway I-80. The first channel, which is closest to the highway, is the virtual source in this record section. The strong asymmetrical NCF suggests that most energy propagates from the highway. The average move-out is about 350 m/s. The phase velocities were determined using the multiple-channel analysis of surface wave methodology. The phase difference due to offset was corrected with frequency and velocity before stacking. The maximum stack energy achieves with optimal phase velocity.

Figure 3 shows that the phase velocities were picked at the maximum of stack energy and shows a clear dispersion from ~500 m/s to ~ 320 m/s between 5 and 15 Hz. The phase velocity dispersion curve is then used to invert for shear wave velocity profiles. A preliminary velocity model at Brady Hot Springs (Lawrence Livermore National Laboratory, 2015) was used as a starting model and the sensitivity kernels of Rayleigh wave group and phase velocities were computed with this model (Figure 4). As the sensitivity kernel shows, shear wave velocity in the top 100 meter can be constrained with Rayleigh wave group and phase velocities in our frequency band.

With the picked phase velocity data, the shear wave velocity structure can be obtained via Occam's inversion (Constable et al., 1987; Lai 1998). Vs gradually increases with depth and it is generally faster than the starting model. Furthermore, the previous model has limited constraints at shallow depth. Logging in well 56-1 suggests that the sediment in the top 30 meters is composed of clay and sandstone, underlain by tuff sediment and tuff between 30 and 100 m depth.

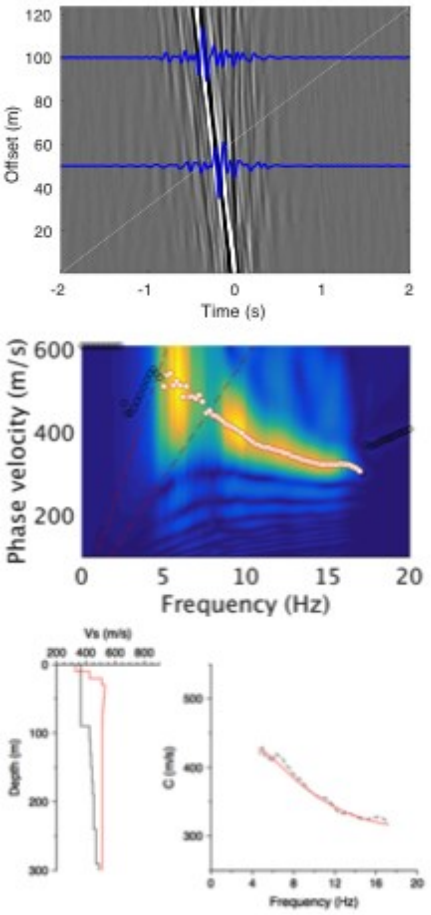

Figure 3. (Top) Record-section of NCFs between channel-pairs along a segment that is perpendicular to highway I-80. The blue lines show two individual NCFs. (Middle) Phase velocities measured with the MASW technique. The red lines show velocity at each frequency that wavelength equals one and half of the length of the segment. The picked velocities are denoted with white circles. (Bottom) Inverted shear wave velocity model (red) and starting model (black, Lawrence Livermore National Laboratory, 2015). The theoretical dispersion curve (solid red line) and picked phase velocities (black dashed line) are shown in right panel.

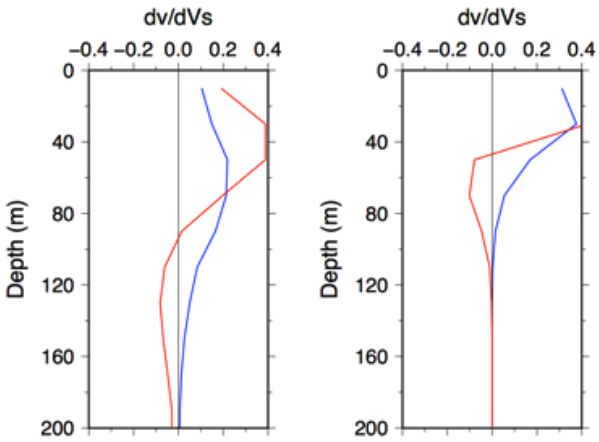

Figure 4. Sensitivity kernels of Rayleigh wave group velocity (red) and phase velocity (blue) at 2 Hz (left) and 5 Hz (right) based on an existing model (Lawrence Livermore National Laboratory, 2015).

The maximum depth of the final model is limited by the lower frequency end of dispersion measurements, which ranges from ~5 Hz to ~10 Hz for the different considered segments. Therefore, we only show the shear wave velocity for the top three layers in Figure 5. The strong spatial variation is interpreted to reflect the different sediments in the near surface. Vs in the northeast corner (X > 300 m and Y > 950 m) is much higher whereas the high-density fractures and high temperature reduce Vs in fault zone (Y = 200 – 1000 m), which is very similar to the results obtained with the geophone dataset (Figure 2).

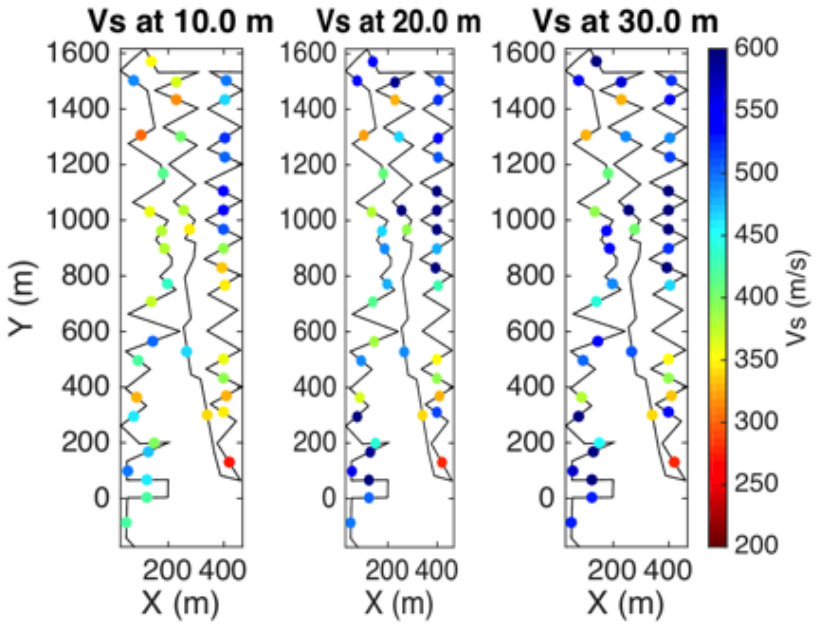

Figure 5. Inverted Vs at different depths. Circle color represents the shear wave velocity. The DAS cable is shown by the black line.

The NCFs of geophones provide dispersion information in a lower frequency band, which can constrain velocity structure at greater depths. The group velocity also provides a different sensitivity kernel, which helps to reduce ambiguity of the inversion. Figure 6 shows result of joint inversion with the two datasets and a new data-driven starting model (Xia et al., 1999). The group velocities in the lower frequency band from the geophone-determined NCF improve resolution at depths greater than 50 m whereas the shallow depths were constrained by higher frequency content afforded by the measurements of the horizontal DAS array and the associated NCFs.

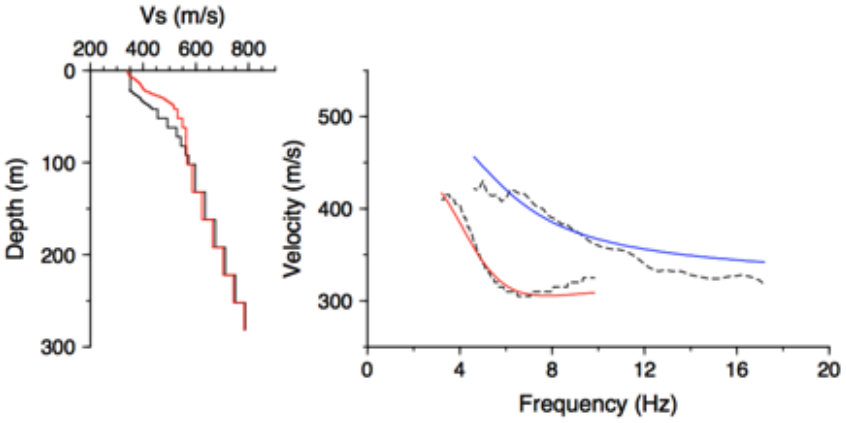

Figure 6. (Left) The new data-driven starting model (black) and final model (red) and (Right) data fitting (dashed lines: observations, solid lines: theoretical values) of joint inversion using geophone and DAS datasets.

4. CONCLUSION

We present the shallow structure revealed by ambient noise tomography using traditional geophone and novel DAS data. The combined results gave surface wave dispersion curves from 2 to 18 Hz, which were used to invert for Vs structure in the top few hundred meters. A low velocity area with a location consistent with the subsidence area from InSAR analysis was revealed with geophone data. Vs in the top few tens of meters obtained from the DAS dataset also reflects different near surface sediments. Joint inversion with the two datasets provides better resolution to greater depth.

The work presented herein was funded in part by the Office of Energy Efficiency and Renewable Energy (EERE), U.S. Department of Energy, under Award Number DE-EE0006760.

REFERENCES

Ali, S. T., Akerley, J., Baluyut, E. C., Cardiff, M., Davatzes, N. C., Feigl, K. L., Foxall, W., Fratta, D., Mellors, R. J., Spielman, P., Wang, H. F., and Zemach, E.: Time-series Analysis of Surface Deformation at Brady Hot Springs Geothermal Field (Nevada) Using Interferometric Synthetic Aperture Radar, *Geothermics*, **61**, (2016), 114-120.

Bensen, G. D., Ritzwoller, M. H., Barmin, M. P., Levshin, A. L., Lin, F., Moschetti, M. P. , Shapiro, N. M. and Yang, Y.: Processing Seismic Ambient Noise Data to Obtain Reliable Broad-Band Surface Wave Dispersion Measurements, *Geophys. J. Int.*, **169**(3), (2007), 1239-1260.

Campillo, M., and Roux P.: Seismic Imaging And Monitoring with Ambient Noise Correlations, in *Treatise on Geophysics*, edited by Romanowicz, B. and A. M. Dziewonski, Elesiver, Amsterdam, **1**, (2014), 256-271.

Constable, S. C., Parker, R. L., and Constable, G. G.: Occam's Inversion: a Practical Algorithm for Generating Smooth Models from Electromagnetic Sounding Data, *Geophysics*, **52**, (1987), 289-300.

Feigl, K. L. and PoroTomo Team: Overview and Preliminary Results from the PoroTomo Project at Brady Hot Springs, Nevada: Poroelastic Tomography by Adjoint Inverse Modeling of Data from Seismology, Geodesy, and Hydrology, *Proceedings*, 42nd Stanford Geothermal Workshop, Stanford University, Stanford, CA (2017).

Lai, C. G.: Simultaneous Inversion of Rayleigh Phase Velocity and Attenuation for Near-Surface Site Characterization. Ph.D. Dissertation, Georgia Institute of Technology (2016).

Lawrence Livermore National Laboratory: PoroTomo_Subtask_3.1:ANT_(initial_waveforms)[data set]. Retrieved from https://gdr.openei.org/submissions/494. (2015), doi:10.15121/1196283.

Wesnousky, S. G., Barron, A. D., Briggs, R. W., Caskey, S. J., Kumar, S., and Owen, L.: Paleoseismic Transect Across the Northern Great Basin, *J. Geophys. Res.*: Solid Earth, **110**(B5), (2005), doi: 10.1029/2004JB003283.

Xia, J., Miller, R. D., and Park, C. B.: Estimation of Near-surface Shear-wave Velocity by Inversion of Rayleigh Waves, *Geophysics*, **64**(3), (1999), 691-700.

Zeng, X., Lancelle, C. Thurber, C., Fratta, D., Wang, H., Lord, N., Chalari, A. and Clarke, A.: Properties of Noise Cross-Correlation Functions Obtained from a Distributed Acoustic Sensing Array at Garner Valley, California, *Bull. Seismol. Soc. Am.*, (2017), doi: 10.1785/0120160168.